REPORT

Visualization of long-lived proteins reveals age mosaicism within nuclei of postmitotic cells

Brandon H. Toyama[1], Rafael Arrojo e Drigo[1], Varda Lev-Ram[2], Ranjan Ramachandra[3], Thomas J. Deerinck[3], Claude Lechene[4], Mark H. Ellisman[3,5], and Martin W. Hetzer[1]

Many adult tissues contain postmitotic cells as old as the host organism. The only organelle that does not turn over in these cells is the nucleus, and its maintenance represents a formidable challenge, as it harbors regulatory proteins that persist throughout adulthood. Here we developed strategies to visualize two classes of such long-lived proteins, histones and nucleoporins, to understand the function of protein longevity in nuclear maintenance. Genome-wide mapping of histones revealed specific enrichment of long-lived variants at silent gene loci. Interestingly, nuclear pores are maintained by piecemeal replacement of subunits, resulting in mosaic complexes composed of polypeptides with vastly different ages. In contrast, nondividing quiescent cells remove old nuclear pores in an ESCRT-dependent manner. Our findings reveal distinct molecular strategies of nuclear maintenance, linking lifelong protein persistence to gene regulation and nuclear integrity.

Introduction

Aging is a physiological condition characterized by an overall decline in organ, cell, organelle, and protein function and homeostasis (Petersen et al., 2003; D'Angelo et al., 2009; Taylor and Dillin, 2011; Blau et al., 2015; Mertens et al., 2015). The negative effects of aging have been well documented in postmitotic tissues, such as the brain and the heart, which contain cells that are as old as the organism itself and are therefore maintained over a lifetime with little to no cellular turnover (Spalding et al., 2005; Bergmann et al., 2009). However, the underlying mechanisms of lifelong persistence and age-dependent decline of these tissues remains poorly understood.

Recently, we have performed ^{15}N stable-isotope pulse-chase labeling of rats followed by cell fractionation and quantitative mass spectrometry of brain and liver tissue to discover proteins with exceptional longevity in neurons that exceed the typical protein lifespan by months or even years (Savas et al., 2012; Toyama et al., 2013). This is in striking contrast to the majority of the proteome, which is renewed within hours or days (Ori et al., 2015). Only a few long-lived proteins (LLPs; i.e., proteins that persist for years) have been previously identified (Fischer and Morell, 1974; Verzijl et al., 2000; Lynnerup et al., 2008). These include eye lens crystalline (Lynnerup et al., 2008), collagen, and myelin basic protein. The latter is a key structural component of myelin, which ensheathes neuronal axons (Fischer and Morell, 1974). The

age-dependent deterioration of these proteins and their role in disease have been studied extensively (Bloemendal et al., 2004; Haus et al., 2007; D'Angelo et al., 2009; Fonck et al., 2009). However, LLPs have not been considered to cause cellular aging, since they reside in extracellular space or in cells that lack metabolic activity (e.g., eye lens; Masters et al., 1977; Shapiro et al., 1991; Verzijl et al., 2000; Bloemendal et al., 2004; Toyama and Hetzer, 2013). Although our ^{15}N metabolic pulse-chase analysis identified many of these same proteins, the approach also revealed a novel set of intracellular LLPs. These LLPs are key components of well-known protein complexes and participate in myriad of cell biological functions, including transcriptional regulation and nuclear trafficking. The lack of turnover of these proteins raises important questions about their role in maintaining cell function over extremely long periods of time within the adult organism. One class of LLPs contains scaffold components of the nuclear pore complex (NPC), and in aged neurons we detected deterioration in nuclear transport activity and loss of the nuclear permeability barrier. This results in the aggregation of cytoplasmic proteins (e.g., tubulin) within the nucleus (D'Angelo et al., 2009). Strikingly, these kinds of intranuclear aggregates have been found in patients with Parkinson's disease (D'Angelo et al., 2009; Woulfe et al., 2010), providing an unexpected link between NPC deterioration and neurodegenerative disorders. Our studies

[1]Molecular and Cell Biology Laboratory, The Salk Institute for Biological Studies, La Jolla, CA; [2]Department of Pharmacology, University of California, San Diego, La Jolla, CA; [3]National Center for Microscopy and Imaging Research, Center for Research on Biological Systems, University of California, San Diego, La Jolla, CA; [4]Division of Genetics, Department of Medicine, Brigham and Women's Hospital, Harvard Medical School, Boston, MA; [5]Department of Neurosciences, University of California, San Diego, La Jolla, CA.

Correspondence to Martin W. Hetzer: hetzer@salk.edu; B.H. Toyama's present address is Celgene Corporation, San Diego, CA.

raise the exciting possibility that the age-dependent functional decline of LLPs might drive cellular alterations that have been observed in aging organs such as the heart and brain.

Nuclear LLPs include the nucleosome core histones H4 and H3.1 and the NPC scaffold nucleoporins (Nups) Nup93, Nup107, and Nup205 (Toyama et al., 2013). Previous data acquired in *Caenorhabditis elegans* and SILAM rats indicate that Nup93 and Nup107 are not replaced once inserted in the nuclear envelope (NE) despite continued protein synthesis, thus suggesting that protein localization may contribute to LLP longevity (D'Angelo et al., 2009; Toyama et al., 2013). This extreme protein longevity presents a challenge to protein homeostasis of LLPs, which are vulnerable to damage accumulation and age-dependent decline in function (Bloemendal et al., 2004; Haus et al., 2007; D'Angelo et al., 2009; Fonck et al., 2009; Toyama et al., 2013). However, the cellular distribution and biological role of LLP longevity and how the overall architecture of nuclei of postmitotic cells, which in humans can last many decades, remains functionally intact are poorly understood.

A recent study used a "fluorescent timer" and time-lapse microscopy to monitor specific protein synthesis and degradation during the cell cycle in mouse embryonic stem cells (Alber et al., 2018). However, to understand NPC maintenance mechanisms (i.e., the relative timing of Nup replacement) in postmitotic cells, we must be able to quantify and experimentally manipulate Nup exchange rates in nondividing cells. Because of the longevity of LLPs, it is not feasible to use FRAP to study them (Ibarra and Hetzer, 2015). Therefore, we established the recombination-induced tag exchange (RITE) system initially developed in yeast (Verzijlbergen et al., 2010), to monitor the replacement of individual Nups in cultured muscle C2C12 cells. This represents an advantage over the ^{15}N system in that the molecular mechanisms underlying Nup exchange can be analyzed in a cellular system suitable for experimental manipulation (e.g., protein mutagenesis, induction of cell stress). In addition, we used our metabolic pulse-chased labeled animals in combination with multi-isotope imaging mass spectrometry (MIMS) to visualize LLPs. Mass spectrometry, even when combined with subcellular fractionation, does not provide information about the precise intracellular localization of identified proteins. Determining the subcellular localization of LLPs will provide important clues concerning the functional relevance of their longevity.

Combining these two methods, we were able to monitor the replacement of specific, long-lived components of NPCs and nucleosomes during aging in postmitotic cells. This led to the observation that postmitotic cells maintain NPC proteins via a piecemeal process. Consistent with our mass spectrometry data, we found that the Nup Pom121 in cultured postmitotic muscle cells is exchanged rapidly, within 2–3 d. In contrast, exchange of Nup93, which is a member of the Nup205 complex, was undetectable over the 2-wk duration of the experiment. Interestingly, two components of the Nup107 complex showed slightly faster, yet different, exchange rates. In contrast, amino acid–deprived quiescent cells are capable of removing old nuclear pores in an endosomal sorting complexes required for transport (ESCRT)–dependent manner. Finally, using genome-wide mapping of long-lived histones revealed specific enrichment of long-lived variants at silent gene loci and thus age mosaicism at the level of chromatin organization.

Results and discussion

Piecemeal replacement of LLPs in postmitotic cells

The previous finding that NPCs in adult neurons are built for life and are not replaced (Toyama et al., 2013; Ori et al., 2015) raised the question about how they are maintained. We speculated that the observed age mosaicism among NPCs is the result of individual Nups being replaced at different and in some cases extremely low rates.

To determine the precise localization and lifespan of these proteins, we adapted a technique called RITE, initially developed to track young and old proteins in yeast (Verzijlbergen et al., 2010). In RITE, the gene of interest is cloned upstream of a C-terminal tag, which is flanked by loxP recombination sites, followed by a different tag (Fig. 1 A). Upon recombination with Cre recombinase, the initial tag is genetically removed and the protein is thereafter translated with the second C-terminal tag. As a consequence, this system allows for the replacement of one tag for another on any protein of interest by a loxP-Cre recombinase system, which ultimately enables the visualization of both young and old versions of the protein. To test this technology, we expressed in U2OS cells a RITE construct with GFP switching to mCherry and were able to visualize replacement of old GFP-labeled proteins by new Cherry-labeled proteins (Fig. 1 B).

Next, we generated RITE switchable epitope tags (Flag to Myc [FM] and Myc to Flag [MF]) of the scaffold NPC proteins Nup93 and Nup96, the intermediately stable Nup133, the short-lived Nup Pom121, and the histones H4, H2B, H3.1, and H3.3 (Jackson, 1990; Kimura and Cook, 2001; Kireeva et al., 2002; Rabut et al., 2004; Toyama et al., 2013). To ensure that each tag did not introduce any localization bias, FM and MF RITE tag versions of each Nup and histone were cotransfected into U2OS cells, and colocalization was confirmed (Fig. S1, A and B). When tag switching was induced in U2OS cells expressing Nup93-FM (details in Materials and methods), old and young versions of the Nup93 protein exhibited distinct localization patterns (Fig. 1 C, bottom row). Similar results were seen with histone H4-FM (Fig. 1 D, bottom row). Because this was done in unsynchronized dividing cells, distinct regions of Nup93 and H4 likely represent the timing within the cell cycle at which tag switch occurred, for example, representing NPCs inserted in early versus late interphase and chromatin replicated early versus late. When these experiments were repeated using tagged versions of Pom121 and histone H2B, two relatively short-lived proteins (Toyama et al., 2013), the distribution of old and young proteins was largely overlapping (Fig. 1, C and D, bottom rows). Therefore, the rapid exchange of Pom121 and H2B suggests that their respective complexes (NPCs and nucleosomes) likely consist of a mixture of young (e.g., Pom121 or H2B) and old (e.g., Nup93 or H4) proteins. Altogether, these results demonstrate that RITE is a powerful approach to visualize the distribution and relative age of proteins within the same cell and that, even in dividing cells, nuclei are mosaics of NPCs with different lifespans (e.g., Pom121 vs. Nup93).
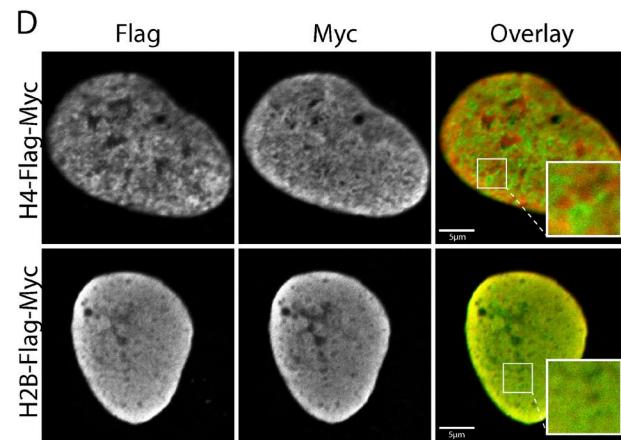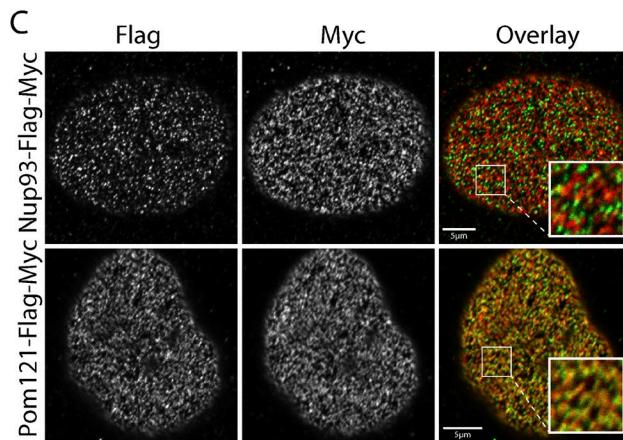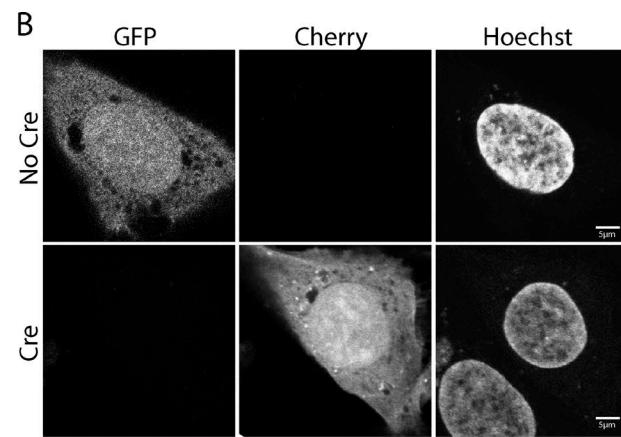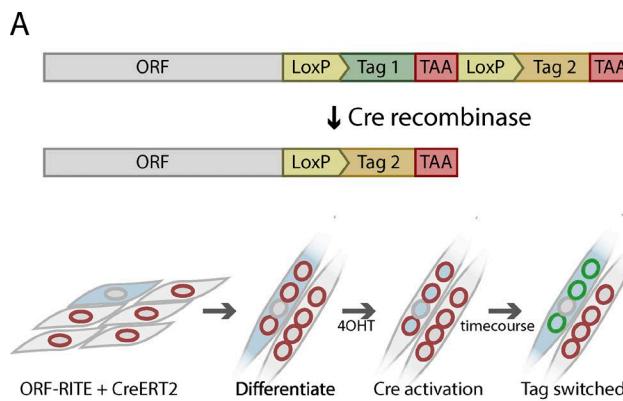
Figure 1. **RITE system for studying protein turnover. (A)** Schematic of the RITE system. Top: The protein of interest (ORF) has a C-terminal tag and stop codon (tag1) flanked by loxP recombination sites, followed by a second tag and stop codon (tag2). Addition of Cre recombinase is used to genetically switch the C-terminal tag to tag2. Bottom: To trigger tag switch in differentiated myotubes, cells expressing RITE-tagged proteins are mixed with cells expressing CreERT2, differentiated to fuse and form myotubes, and tag-switch induced by the addition of 4OHT. **(B)** RITE system in mammalian cells. Dividing U2OS cells expressing a GFP-cherry RITE construct were fixed and imaged before (upper) and 3 d after (lower) Cre addition. **(C)** NPC proteins RITE-tagged. Dividing U2OS cells were transfected with RITE-tagged (FM) Pom121 and Nup93 nucleoporins, tag switch induced, fixed and stained 16 h later, and imaged by confocal microscopy. Inset represents a zoomed-in view of the region indicated. **(D)** Histones RITE-tagged. Histones H2B and H4 were RITE-tagged, expressed, fixed, stained, and imaged as in B. Scale bars represent 5 μm.

Long-lived histones localize to the heterochromatin

In our previous studies, we identified a subset of histones to be long-lived and wondered whether age mosaicism is a feature of chromatin organization. We therefore decided to test whether nucleosomes in dividing and nondividing cells might also exhibit age mosaicism. To do this, we used the C2C12 differentiation system, in which cells can exist in (a) a dividing myoblasts state, (b) a quiescent state where cells are poised to reenter the cell cycle, or (c) a nondividing terminally differentiated myotube state that, like neurons, do not reenter the cell cycle. Because myotubes result from the fusion of myoblasts to form multinucleated tubules, we mixed RITE-tagged myoblasts with a small number of myoblasts expressing inducible Cre-ERT2 and used the addition of 4-hydroxytamoxifen (4OHT) to initiate tag-switch, ensuring that the switch occurred only in cells that underwent fusion and terminal differentiation (Fig. 1 A). To achieve this, we expressed RITE-tagged histones H2B, H3.1, H3.3, and H4 in C2C12 cells and followed their turnover after tag-switch in dividing or quiescent myoblasts and postmitotic myotubes. As expected, in dividing myoblasts, all four histones exhibited almost complete turnover after 1–2 d (Fig. 2 A). In nondividing myotubes (Fig. 2 B) and quiescent cells (Fig. 2 C), however, some histone H3.1, H3.3, and H4 persisted for 7 d, concentrating around nuclear foci. Because histone H3.1 is associated with heterochromatin, and previous studies have suggested that heterochromatic histones are long-lived (Hake et al., 2006; Aygün et al., 2013), we hypothesized that these foci of old histones corresponded to heterochromatin. To test this, we costained with the constitutive heterochromatin mark H3K9me3 and found that 7-d-old histones indeed localized to foci of heterochromatin (Fig. 2, B and C), consistent with the lack of histone turnover observed in heterochromatic regions in dividing yeast (Aygün et al., 2013).

To extend this analysis genome-wide, we performed chromatin immunoprecipitation sequencing (ChIP-seq) targeting old or new histone H3.3 and H3K9me3 in nondividing myotubes at 0 or 7 d after tag-switch induction with 4OHT. This analysis revealed that new H3.3 preferentially incorporated into regions of active chromatin which lack H3K9me3 (Fig. 2 C), consistent with previous work demonstrating that histone turnover is coupled to transcription (Mito et al., 2005; Maze et al., 2015). Thus,
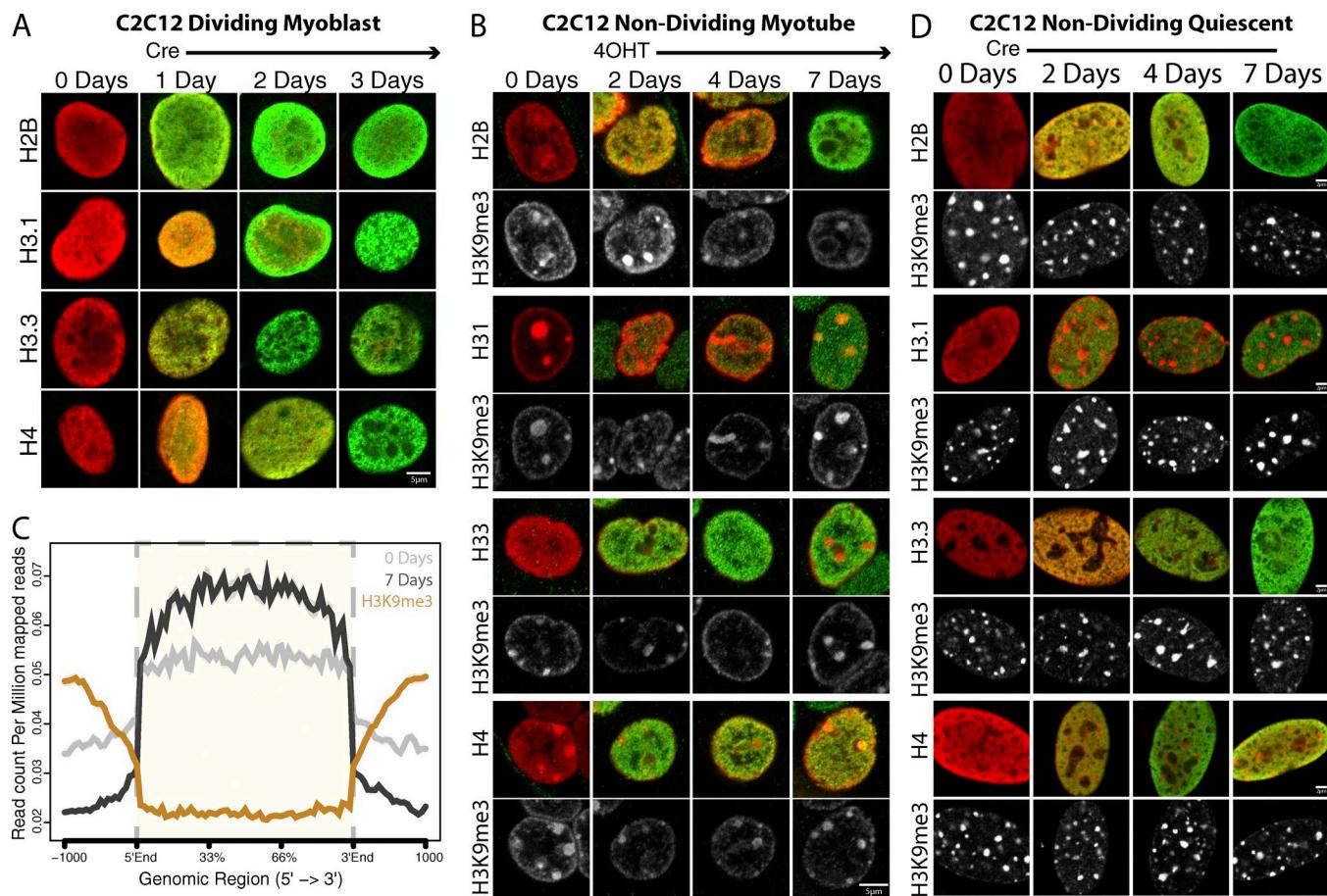
Figure 2. **Histone dynamics using the RITE system. (A)** Histone turnover in dividing cells. C2C12 cell lines stably expressing RITE-tagged (MF) H2B, H3.1, H3.3, and H4 were made, fixed, stained, and imaged using confocal microscopy before (0 Days) and 1, 2, and 3 d after tag switch was initiated in dividing cells. Representative images are displayed with Myc signal (red) overlaid with Flag signal (green). **(B)** Histone turnover in nondividing myotubes. The same cells from A were differentiated into myotubes as outlined in Fig. 1 A and fixed, stained, and imaged before (0 d) and 2, 4, and 7 d after tag switch. Upper panel of each set is the Myc (red) overlaid with Flag (green) signal. Lower panel of each set is staining of H3K9me3 in the same cells. Scale bars represent 5 μm. **(C)** ChIP-seq of RITE-tagged H3.3. RITE-tagged (MF) H3.3 C2C12 cells were differentiated into myotubes as described above and tag-switch induced. Myotube-enriched fractions were isolated from cells with no tag switch (0 d) and tag switched for 2 and 7 d. ChIP-seq was then performed on these time points using anti-Flag and anti-H3K9me3 antibodies. Regions of flag-tagged H3.3 incorporation were identified genome-wide (5′ to 3′ end), and H3K9me3 reads were correspondingly mapped. **(D)** Histone dynamics in quiescent cells. C2C12 cell lines from this figure were placed in quiescence, and tag switch time courses, staining, and imaging were conducted as described for B.

in nondividing cells, exchange rates of histones correlated with the type of underlying chromatin marks, with active chromatin harboring short-lived histones and inactive chromatin occupied by long-lived histones. These results show that protein age mosaicism is a feature of long-term genome maintenance, whereby chromatin is composed of nucleosomes with vastly different lifespans.

NPC turnover in dividing and postmitotic cells

Previous experiments in *C. elegans* and rats revealed that LLPs can persist for months in tissues with limited regenerative capacity, such as the brain (D'Angelo et al., 2009; Savas et al., 2012; Toyama et al., 2013; Ori et al., 2015). This raised the question of how these protein assemblies are maintained in nondividing cells over such long periods of time. For example, it is unclear whether the stable scaffold of the NPC is turned over by replacing the entire scaffold at once, or by slowly replacing individual subcomplexes (i.e., Nup93) within the NPC scaffold. In addition,

are all NPCs within a given cell identical in age, or are there NPCs of different ages within each cell?

We therefore wanted to study this remarkable protein stability using RITE in a postmitotic cell system in vitro. Specifically, we wanted to visualize NPC protein exchange rates at the NE. To study Nup dynamics in dividing myoblasts and nondividing myotubes, we RITE-tagged two stable Nups (Nup93 and Nup96), an intermediately stable Nup (Nup133), and a dynamic Nup (Pom121) and expressed them separately in C2C12 cells. In dividing myoblasts, all four RITE-tagged Nup proteins were turned over at similar rates, generally within 2 d (Fig. 3 A). When the same cells were differentiated into nondividing myotubes, however, Nup93 and Nup96 exhibited very little turnover, whereas Nup133 and Pom121 exhibited moderate (50% after 2 wk) and rapid (75% after 2 wk) levels of turnover, respectively (Fig. 3 B), recapitulating the age mosaicism seen across different components of the NPC in the rat (Toyama et al., 2013). Cells expressing Nups with FM and MF RITE-tagged versions were also mixed and
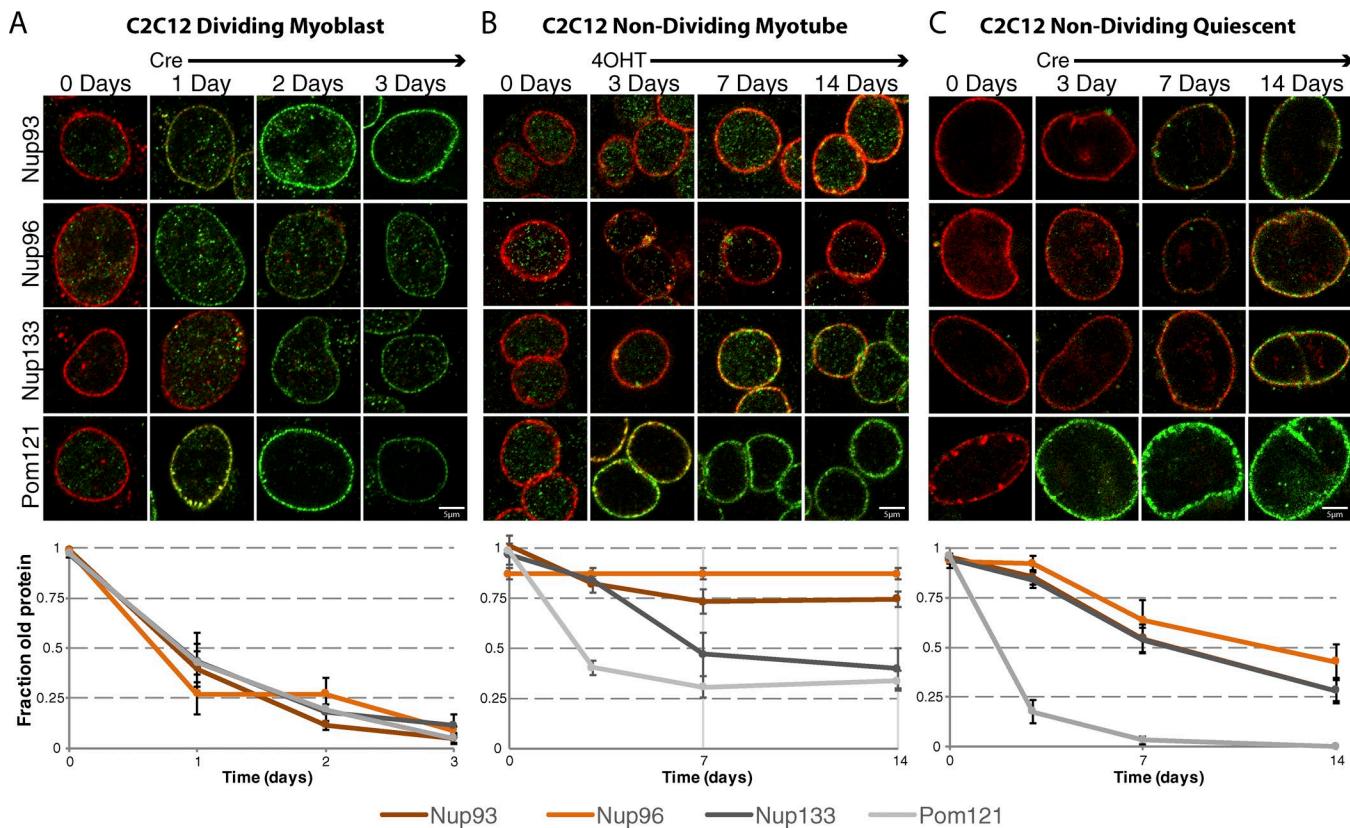
Figure 3. NPC dynamics using the RITE system. (A) Nups in dividing C2C12s. C2C12 cell lines stably expressing RITE-tagged (MF) Nup93, Nup96, Nup133, and Pom121 were made, fixed, stained, and imaged using confocal microscopy before (0 Days) and 1, 2, and 3 d after tag switch was initiated in dividing cells. Representative images are displayed with Myc signal (red) overlaid with Flag signal (green). Quantification of NE-localized Nup-RITE proteins, plotted underneath, is of relative Myc intensity on the NE as a fraction of total (MF) intensity on the NE. **(B)** Nups in nondividing myotubes. Cell lines from A were differentiated into nondividing myotubes as described in Fig. 1 A and fixed, stained, and imaged before (0 Days) and 3, 7, and 14 d after tag switch. Image representation and quantification are as described in A. **(C)** Nups in nondividing quiescent cells. Cell lines from A were induced into quiescence, fixed, stained, and imaged before (0 Days) and 3, 7, and 14 d after tag switch. Image representation and quantification are as described in A. All scale bars represent 5 μm. Error bars represent the 95% confidence interval.

differentiated, resulting in myotubes that express both tags simultaneously. Similar stability (Nup93 and Nup96) and turnover (Nup133 and Pom121) were seen, demonstrating that the diverse dynamics are not an artifact of Cre or 4OHT (Fig. S1 C). These findings strongly support the idea that NPCs are built to last the entire life of a cell.

Next, we studied Nup dynamics in quiescent muscle cells, where we expected results similar to those in postmitotic myotubes. However, new Nup93 and Nup96 incorporated into quiescent nuclei at significant rates (50% after 2 wk; Fig. 3 C). The appearance of newly synthesized Nup93 and Nup96 was not due to cell division, as we determined the quiescent status of these cells by thymidine analogue EdU incorporation and use of the cycling cell poison cytosine arabinoside (AraC; Fig. S1, D–F). Furthermore, total NPC number also did not change substantially over 28 d, showing that the new protein incorporation we observed in quiescent cells was not simply due to the addition of new nuclear pores (Fig. S2 B). Taken together, these data suggested that for every new NPC inserted, an old NPC must be removed. To explore this phenomenon further, we used the RITE system to visualize Nup exchange at the single-pore level using structured-illumination microscopy (SIM; Fig. 4, A and B). If NPC turnover in quiescent

cells occurs through subcomplex turnover, we would expect each pore to have a mixture of old and new scaffold proteins. However, if turnover occurs through whole-pore turnover, we would expect each NPC to contain old or new scaffold proteins, but not both (Fig. S2 A). SIM superresolution imaging of RITE-tagged NPC proteins showed that the vast majority of both old and new proteins, at 7 and 14 d after tag-switch, were clearly visible and their localization patterns did not overlap (Figs. 4 A and S2, C and D). These data strongly suggest that entire NPCs are removed from the NE and replaced by new ones. Consistent with this idea, the number of old NPCs decreased and the number of new NPCs increased (Fig. 4 B), whereas the total NPC density remained constant (Fig. S2 E). Notably, we observed a small amount of overlap between old and new proteins (Figs. 4 and S2, C and D), suggesting that rare piecemeal replacement events of specific NPC components may also take place. These results indicate that NPC maintenance occurs by distinct mechanisms in terminally differentiated cells and in quiescent cells: although NPCs in postmitotic cells can last an entire lifetime and are maintained by piecemeal replacement (and reincorporation) of individual components at different rates, NPCs in quiescent cells are turned over as one entire unit, similar to ribosomes (Retz and Steele, 1980).
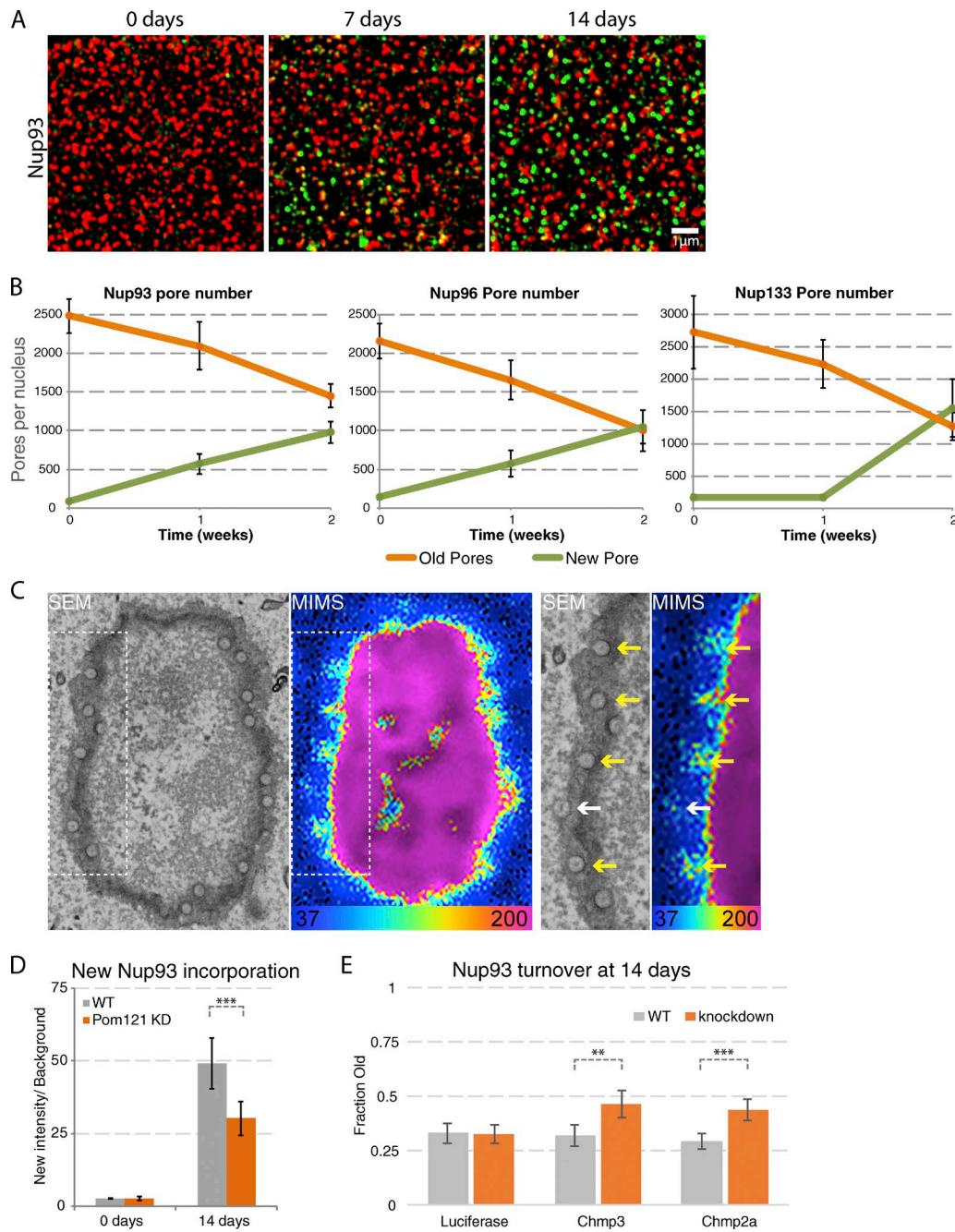
Figure 4. **Mechanism of NPC turnover in nondividing quiescent cells. (A)** Single pore imaging of Nup93 turnover in quiescent cells. C2C12 cells stably expressing RITE-tagged (MF) Nup93 were induced into quiescence and tag switch initiated. Cells were fixed and stained before (0 Days) and 7 and 14 d after tag switch. Cells were then imaged using structured illumination superresolution microscopy. Representative images display Myc (red) and Flag (green) signal overlaid. Scale bar represents 1 µm. **(B)** Quantification of Nup turnover in quiescent cells. Identical experiments were performed using Nup96 and Nup133 as described in A. Myc (Old) and Flag (New) pore numbers were then quantified at each time point and plotted. Error bars represent 95% confidence intervals. **(C)** MIMS imaging of long-lived NPCs. ^{15}N-labeled mice chased with ^{14}N food for 6 mo were perfused and fixed, tissues dissected and prepared for EM, and 80-nm-thick brain sections mounted on silicon wafers were imaged by scanning EM (SEM; left) and MIMS (right). Images were aligned, NPCs identified in SEM images (arrows), and corresponding MIMS signals highlighted (arrows). Yellow arrows represent NPCs with high ^{15}N signal, and the white arrow is an NPC with low ^{15}N signal. Data shown is from one mouse and is representative of three scanned neurons. **(D)** Nup93 turnover in Pom121 knockdowns. C2C12 cell lines were constructed that expressed both RITE-tagged (MF) Nup93 and an inducible shRNA targeting Pom121. Cells were placed into quiescence and tag switch induced with (orange bars) and without (gray bars) Pom121 knockdown induction. Cells were fixed, stained, and imaged before (0 Days) and 14 d after tag switch. Intensity of the flag signal (new) was normalized to background intensity and plotted. Error bars represent 95% confidence intervals. **(E)** Nup93 turnover with ESCRT-III knockdowns. C2C12 cell lines were constructed as in D, but expressing a nontargeting (luciferase) or ESCRT-III targeting inducible shRNAs (Chmp3 and Chmp2a). Turnover was quantified as described in Fig. 3 A. **, P < 0.01; ***, P < 0.001 calculated using two-tailed unpaired t tests.

Toyama et al.
Age mosaicism within nuclei of postmitotic cells

Journal of Cell Biology 438
https://doi.org/10.1083/jcb.201809123

Imaging NPC turnover in vivo

To determine whether this type of NPC age mosaicism is present in vivo and to determine the age of individual NPCs in the brain of mice, we used correlated MIMS (Zhang et al., 2012) and scanning EM (herein called MIMS-EM). MIMS is an isotope mapping technology that uses a scanning cesium beam to ionize different isotopes (e.g., ^{15}N and ^{14}N) embedded in a cell or large protein complex and that are then detected by different mass detectors (Zhang et al., 2012). As a result, MIMS generates quantitative and ratio-metric isotope maps (displayed here as a ^{15}N-to-^{14}N ratio [$^{15}N/^{14}N$]) that are combined with scanning EM to provide high-resolution structural information overlaid with age. Here, using a similar approach to the one used to discover LLPs (Toyama et al., 2013), we generated a mouse labeled in utero and throughout early life with ^{15}N until postnatal day 45 (P45) and chased for 6 mo. This labeling approach labels amino acids and nucleic acids with ^{15}N, and after 6 mo of chase, most of the ^{15}N signal that remains in neurons is nuclear and is from DNA and rare LLPs (i.e., embedded NPCs and core histones), as expected (Fig. S3 A; Savas et al., 2012; Toyama et al., 2013). Next, we imaged en face neuronal NPCs from a single neuron located in layer 2 of the primary cortex and observed that four of five NPCs imaged contained $^{15}N/^{14}N$ levels that ranged between 1.5- and 3-fold above the natural ratio (Fig. 4 C). However, although this NPC ^{15}N-positive signal was not present in neighboring areas of the NE that did not contain NPCs (Fig. S3 A), it was possible that the observed NPC ^{15}N signal could be from the underlying ^{15}N-rich heterochromatin (Fig. S3 B). Therefore, we took advantage of nucleus curvature and applied MIMS-EM to serial sections from the "cap" of another neuron nucleus (Fig. S3, B and C), allowing us to image NPCs in the Z-axis and to minimize the risk of contamination from underlying heterochromatin. Reconstruction of the MIMS-EM data stack revealed that most NPCs are long-lived and contained ^{15}N levels three times above the natural ratio (Fig. S3, A and C). We also observed rare NPCs that did not retain ^{15}N above background levels (Fig. 4 B and Fig. S3, A [magenta arrows] and C [lower panel]). These results strongly support the idea that most NPCs in LLCs are indeed long-lived structures with components that can last at least 6 mo and confirm our previous findings (Toyama et al., 2013). Strikingly, these data suggest that the turnover and/or maintenance of NPC-associated LLPs is heterogeneous and highlight a potential age mosaicism among different NPCs of the same nucleus.

NPC turnover in quiescent cells is Pom121 and ESCRT dependent

Although we observed NPC turnover occurring in quiescent cells, how might the addition and removal of entire NPCs from the intact NE occur in the absence of cell division? In dividing cells, NPC assembly requires the transmembrane Nup Pom121 (Antonin et al., 2005; Doucet et al., 2010). To determine whether new NPC insertion in quiescent cells occurs through a similar mechanism, an inducible shRNA system was used to selectively knock down Pom121 at tag-switch initiation (Fellmann et al., 2013). Indeed, NPC insertion was markedly decreased in cells with reduced levels of Pom121, compared with uninduced controls (Fig. 4 D). But how are entire NPCs removed from the intact NE without

disrupting nuclear/cytoplasmic compartmentalization? One potential mechanism would be autophagy of a portion of the NE, including resident NPCs, as nucleophagy has been observed in yeast (Roberts et al., 2003; Kvam and Goldfarb, 2007). Next, we quantified NPC turnover in quiescent cells in the presence of the autophagy inhibitor 3-MA or the autophagy activator trehalose (Sarkar et al., 2007; Yang et al., 2013); however, no significant effect was observed in treated cells (Fig. S3, D and E).

An alternative means by which NPCs could be turned over is through ESCRT complexes, as this pathway mediates NE resealing following mitosis and removal of aberrant or incomplete NPCs from the intact NE (Webster et al., 2014; Olmos et al., 2015). To test this, we established Nup93-RITE cell lines with doxycycline-inducible shRNAs to knockdown the ESCRT-III proteins Chmp3, Chmp2a, or a luciferase control. Induction of the shRNA resulted in knockdown of the corresponding proteins (Fig. S3, F and G) and partially inhibited Nup93 turnover in the ESCRTI II, but not luciferase, shRNA cell lines (Fig. 4 E). These findings suggest a role for the ESCRT machinery in quiescent cells and suggest that topological NE remodeling events may be involved in NPC removal in quiescent cells.

Age mosaicism of proteins and protein complexes has largely been an unexplored area of research. In this study, we were able to define the spatial organization and rationale for age mosaicism within single cells. Our data indicate that the age of a protein may define or be necessary for an underlying function, such as the maintenance of silent heterochromatin by old histones. For the NPC, age mosaicism is twofold, as it occurs within the same complex between different proteins, and across different NPCs within the same cell. As the NPC participates in genome organization, gene regulation, and transport into and out of the nucleus, determining whether old versus young NPCs mediate distinct functions will be a complex but exciting area of future research. The NPC is a good example for this molecular-age mosaicism, since individual nucleoporins in the same protein complex have different lifespans. Our studies reveal that this mosaicism can be explained by a slow piecemeal replacement mechanism that allows NPCs to be maintained over long periods of time. This supports the idea of a piecemeal maintenance mechanism by which specific NPC components and the NPC structure can persist for the lifespan of a cell but is composed of relatively younger components. More broadly, the RITE system will help identify and functionally characterize other examples of protein-age mosaicism.

Materials and methods

Plasmid and strain construction

The GFP-Cherry RITE cassette was constructed with a 3xGGS linker (5′-GGAGGCTCGGGGGGCAGCGGAGGCTCGGGG-3′) followed by a loxP recombination sequence (5′-ATAACTTCGTAT AATGTATGCTATACGAAGTTATCA-3′), BamH1 cut site, eGFP, BamH1 cut site and stop codon, loxP sequence, Age1 cut site, mCherry sequence, Age1 cut site, and stop codon. The Myc-Flag cassette was constructed with the 3xGGS linker, loxP site, 3xMyc tag separated by GGS linkers (5′-GAGCAGAAACTCATCAGCGAA GAAGATCTCGGGGGATCCGAACAAAAGCTTATCTCCGAAGAG

GATCTGGGTGGTAGTGCATCAATGCAGAAGCTGATCTCAGAG
GAGGACCTG-3'), stop codon, loxP site, 3xFlag tag separated by
GGS linkers (5'-GATTACAAGGATGACGACGATAAGGGGGGATCC
GACTACAAAGACGATGATGACAAAGGTGGTAGTGATTACAAG
GATGACGACGATAAG-3'), and stop codon. The FM cassette was
constructed as above, but with the 3xMyc and 3xFlag sequences
swapped. All three were initially cloned into the pEGFP-N1 (Clon-
tech) vector at the SacII/NotI sites. GFP-Cherry control was made
by inserting the Myc sequence as the ORF. Sequences for the
human versions of Nup93; Nup96; Nup133; Histone H2B, H3.1,
H3.3, and H4; and the rat sequence for Pom121 were all cloned
into the FM and MF constructs, and these sequences with the
RITE constructs were then cloned into pDONR207 plasmids
using Gateway cloning (Thermo Fisher Scientific). Gateway con-
structs were then recombined into lentiviral vectors ([Campeau et
al., 2009](#)) marked with blasticidin (pLentiCMVBlast) or puromy-
cin (pLentiCMVPuro), and third-generation lentivirus protocols
were followed to produce virus in 293T cells. C2C12 cells were
infected with viral supernatant from 293T cells in the presence
of 6 µg/ml polybrene for 24 h and selected 48 h after infection
with either 10 µg/ml blasticidin or 2 µg/ml puromycin.

shRNA construction and cell lines
shRNAs were designed targeting mouse Pom121, Chmp3, and
Chmp2a using the shERWOOD algorithm ([Knott et al., 2014](#)) and
cloned into the EcoRI and XhoI sites in the mIR-E lentiviral all-
in-one plasmid ([Fellmann et al., 2013](#)). Sequences used were as
follows: Pom121, 5'-TGCTGTTGACAGTGAGCGACAGGAGAAAAG
GTTACAGATATAGTGAAGCCACAGATGTATATCTGTAACCTTTTC
TCCTGGTGCCTACTGCCTCGGA-3'; Chmp3, 5'-TGCTGTTGACAG
TGAGCGCGAAGAGCACAGAAGTGATGAATAGTGAAGCCACAG
ATGTATTCATCACTTCTGTGCTCTTCTTGCCTACTGCCTCGGA-3';
and Chmp2a, 5'-TGCTGTTGACAGTGAGCGAATGGGTGATGAGGA
AGATGAATAGTGAAGCCACAGATGTATTCATCTTCCTCATCACCC
ATGTGCCTACTGCCTCGGA-3'. Cell lines expressing the inducible
shRNAs were made in blasticidin-selected Nup-RITE C2C12 cell
using puromycin to select for the shRNA.

Antibodies and imaging reagents
All antibodies were used at 1:1,000 dilution unless otherwise
indicated. Mouse anti-Myc (9B11; Cell Signaling Technolo-
gies), mouse anti-Flag (M2; Sigma), and rabbit anti-H3K9me3
(ab8898; Abcam) antibodies were used for all immunofluores-
cence and ChIP experiments. Mouse Mab414 (ab50008; Abcam)
was used for NPC staining and pore counting by superresolu-
tion microscopy. Rabbit anti-Chmp3 (PA5-49400; Invitrogen),
rabbit anti-Chmp2a (GTX102142; GeneTex), and mouse anti-
GAPDH (ab8245; Abcam) were used for Western blotting. For
imaging Myc and Flag simultaneously, Alexa Fluor 488 goat
anti–mouse IgG1 (A21121; Thermo Fisher Scientific) and Alexa
Fluor 568 goat anti–mouse IgG2a (A21134; Thermo Fisher Sci-
entific) secondary antibodies were used. For H3K9me3 stain-
ing, Alexa Fluor 647 goat anti–rabbit secondary antibody was
used. For Western blots, HRP anti-mouse and -rabbit second-
ary antibodies were used at 1:5,000 dilutions. For EdU imag-
ing, the Click-iT EdU Alexa Fluor 555 imaging kit and protocol
were used (C10338).

Cell culture and RITE tag switching
U2OS cells were cultured in DMEM with 10% FBS in the pres-
ence of penicillin streptomycin (P/S) antibiotics. Dividing C2C12
cells were cultured in DMEM, 20% FBS, and P/S. For differentia-
tion into myotubes, C2C12 cells were normally grown until fully
confluent, washed with warm PBS and warm DMEM, with 2%
horse serum and P/S medium added (myotube medium). Cells
were kept in myotube medium for 5 d to differentiate, and time
course experiments started with that day as the time = 0 point,
unless otherwise stated. Myotube medium was changed every 2
d throughout the time course. Tag switch was initiated by add-
ing 4OHT (H6278; Sigma) to 1 µM concentration for 24 h. Quies-
cent cells were induced based on previously described methods
([Zhang et al., 2010](#)) by growing C2C12 myoblasts to ∼75% con-
fluence, washing twice with warm PBS, and adding quiescent
medium (DMEM without methionine, 2% FBS, and P/S). Cells
were kept in quiescent medium for 3 d, after which time course
experiments were started as that day as time = 0. Quiescent me-
dium was changed every 2 d. For tag exchange in U2OS, C2C12
myoblasts, and quiescent cells, concentrated adenovirus express-
ing Cre (Ad-Cre) was added to the medium (University of Iowa).

RITE in U2OS
For [Figs. 1 B](#) and S1, GFP-Cherry and Nup93, Nup96, Nup133,
Pom121, H2B, H3.1, H3.3, and H4 RITE-tagged constructs (FM and
MF) were transiently transfected into U2OS cells on coverslips
according to the manufacturer's protocol using Lipofectamine
2000 (Thermo Fisher Scientific). For [Fig. 1 B](#), tag switch was ini-
tiated 3 d before fixing. 2 d after transfection, Nup-transfected
cells were preextracted by washing with CSK buffer (10 mM
Pipes, pH 7, 100 mM NaCl, 300 mM sucrose, and 3 mM MgCl$_2$) at
4°C, and then incubated with CSK buffer with 0.5% Triton X-100
(CSK-T) at 4°C for 5 min. Cells were immediately fixed with 4%
PFA (Electron Microscopy Sciences) for 2 min at RT. 2 and 4 d,
respectively, after transfection, histone and GFP-Cherry trans-
fected cells were washed with PBS and fixed in 4% PFA at RT for 2
min. All fixed cells were then solubilized and blocked in IF buffer
(0.1% Triton X-100, 0.02% SDS, and 20 mg/ml BSA, in PBS) at RT
and stained for Myc and Flag in IF buffer for 1 h at RT, washed
three times in IF buffer, stained with secondary antibodies in IF
buffer for 1 h at RT, and washed three times in IF buffer. For [Fig. 1
(B–D)](#) and Fig. S1 B, cells were mounted in Vectashield and sealed
before imaging using confocal microscopy (LSM710; Zeiss). For
Fig. S1 A, cells were initially seeded on high-performance cover
glass (474030-9000-000; Zeiss) and, after fixing and staining
as described above, mounted using ProLong Gold (P36930; Life
Technologies), allowed to cure at RT for 3 d, and imaged using
Airyscan superresolution microscopy (LSM 880; Zeiss).

RITE in myoblasts
Stable C2C12 cell lines expressing Nup93, Nup96, Nup133, Pom121,
H2B, H3.1, H3.3, and H4 with FM and MF RITE tags were made and
grown on coverglass. 16 h before fixing, tag-switch was initiated
by Ad-Cre virus. Nup cell lines were preextracted as described
above, and both Nup and histone cell lines were fixed and stained
as described above. Mounting and imaging was performed as de-
scribed above using confocal microscopy (LSM710). Fluorescence

Toyama et al.
Age mosaicism within nuclei of postmitotic cells

Journal of Cell Biology 440
https://doi.org/10.1083/jcb.201809123

was quantified by adjusting laser power and gain settings on the 0-d and final-day time points to ensure maximum signal without saturation. All time points were then imaged using identical settings, and mean intensity signal for Myc and Flag was determined for each cell using ImageJ (National Institutes of Health). Fraction intensity was calculated as old intensity minus background, divided by old plus new intensity minus background.

RITE in myotubes for imaging

Stable C2C12 cell lines from above were individually grown to confluence at a 5:1 ratio with a stable C2C12 cell line expressing CreERT2 in Ibidi μ-Slide chambers (80826; Ibidi). Myotube induction was performed as described above. Tag switch at the indicated time points was initiated at the respective days before fixation. The entire slide (all time points) was then fixed and stained as described above. Imaging and quantification were performed as described above. For analyzing Nup turnover without using Cre or 4OHT (Fig. S1 C), indicated (FM and MF) Nup cell lines were mixed and differentiated as described above. No tag switch was initiated. After 14 d in myotube media, cells were fixed, stained, and imaged as described above.

RITE in quiescent cells

Stable C2C12 cell lines from above were grown in Ibidi chamber slides and put into quiescence medium as described above. Tag switch at the indicated time points was initiated at their respective days before fixation, and the entire slide (all time points) fixed, stained, imaged, and quantified as described above. For experiments expressing shRNAs, C2C12 cell lines with the Nup-RITE and shRNAs described above were left untreated (no dox) or treated with 1 μg/ml doxycycline (50328702; Thermo Fisher Scientific), with drug addition occurring simultaneously with tag-switch. 3-Methyl adenine at 5 mM (3MA; M9281; Sigma), trehalose 100 mM (T9531; Sigma), and cytosine arabinoside at 10 μM (AraC; Sigma) were all added at tag-switch and remained in culture throughout the rest of the experiment. To identify DNA synthesis in quiescence (Fig. S1 C), cells were placed in quiescence medium as described above, and 24 h before the indicated time points, EdU was added to 10 μM. For Fig. 3 C, EdU was added to 10 μM for the entire (14-d) time course, and tag switch was induced as described above. For rich medium add-back, quiescence medium was removed and replaced with myoblast medium 24 h before fixing and staining. For superresolution imaging, experiments were performed as described above, but with cells seeded on high-performance cover glass, fixed, stained, mounted as described in RITE in U2OS above, and imaged using superresolution SIM (Elyra PS.1; Zeiss).

Image analysis

Fraction Myc or Flag intensities were calculated by determining signal intensity of NPC-localized protein by quantifying signal at the NE using Fiji (ImageJ). Background intensity values were then subtracted for each image, and fraction intensity was calculated as the old protein intensity divided by the old plus new signal intensities. To calculate new protein incorporation, only new protein intensities with background subtracted were determined and plotted. Quantification of NPC numbers was done on 3D-reconstructed SIM images using the spot finder and surface tools (Imaris, Bitplane). Statistics were calculated using two-tailed unpaired t tests (Prism; GraphPad). Colocalization plots and analysis were performed using Imaris (v9.2; Bitplane) and displayed Mander's correlation coefficients represent calculated values after automatic thresholding. For Figs. S1 A and S2 C, point spread function width = 0.115 μm. For Fig. S1 B, point spread function width = 0.396 μm. Numbers of nuclei quantified are as follows: Fig. 3 A, Nup93 (19, 19, 31, 32), Nup96 (5, 8, 16, 22), Nup133 (15, 8, 12, 10), Pom121 (10, 19, 23, 14); Fig. 3 B, Nup93 (24, 29, 26, 26), Nup96 (10, 16, 10, 18), Nup133 (14, 10, 16, 12), Pom121 (15, 30, 41, 28); Fig. 3 C, Nup93 (26, 19, 28, 29), Nup96 (11, 6, 13, 10), Nup133 (15, 18, 36, 39), Pom121 (19, 20, 13, 5); Fig. 4 B, Nup93 (10, 11, 11), Nup96 (11, 12, 13), Nup133 (10, 9, 11); Fig. 4 D, 0 d (28, 23), 2 wk (32, 38); Fig. 4 E, Luciferase (20, 16, 28, 26), Chmp3 (12, 23, 15, 13), Chmp2 (25, 16, 18, 20); Fig. S2 E, same as Fig. 4 B; Fig. S3 B, Nup93 0 d (8, 4), 14 d (10, 2), Nup96 0 d (6, 4), 14 d (8, 3), Nup133 0 d (8, 8), 14 d (23, 3), Pom121 0 d (8, 4), 4 d (13, 7); and Fig. S3 C, Nup93 0 d (24, 18), 7 d (15, 25), Nup96 0 d (19, 20), 7 d (20, 22).

ChIP-seq of RITE in myotubes

A stable C2C12 cell line expressing RITE-MF–tagged histone H3.3 was cultured and differentiated into myotubes as described above, using one 15-cm plate per immunoprecipitation (IP) per time point. Tag switch was initiated as described above using 4OHT or left untreated for the 0-d time point. At 2, 4, and 7 d after tag switch (2 d for untreated), cells were washed once with PBS and incubated with 1:5 diluted trypsin/versene solution at 37°C. Cells were carefully monitored until differentiated myotubes came off the plate and single-cell quiescent cells remained attached (5–10 min), trypsin was quenched by adding myotube medium, and all myotubes were collected from the plate. Cells were pelleted, washed with 1× PBS, and resuspended in 1% formaldehyde in PBS for 10 min at RT. Glycine was added to 125 mM final concentration, cells were pelleted at 4°C, and pellets were snap-frozen. For chromatin shearing, pellets were resuspended in CiA NP1 (50 mM Hepes, pH 8.0, 140 mM NaCl, 1 mM EDTA, 10% glycerol, 0.5% NP-40, and 0.25% Triton X-100) at 4°C for 5 min, nuclei were pelleted at 1,200 relative centrifugal force for 5 min at 4°C, and pellet was washed similarly by resuspending and spinning with CiA NP2 (10 mM Tris, pH 8.0, 1 mM EDTA, 0.5 mM EGTA, and 200 mM NaCl) and twice with Covaris shearing buffer (0.1% SDS, 1 mM EDTA, and 10 mM Tris, pH 8.0). The final pellets were resuspended in 130 μl Covaris shearing buffer with 1× protease inhibitors (Complete EDTA-free; Roche), and sheared in AFA fiber microTUBE tubes (520045; Covaris) in a E220 machine (Covaris) for 20 min (2% duty, 105 Watts, 200 cycles per burst, 4°C). Sheared chromatin was spun at 4°C for 5 min, and supernatant was kept for IP, with 10% set aside for input DNA. 5× IP buffer (250 mM Hepes, pH 7.5, 1.5 M NaCl, 5 mM EDTA, 5% Triton X-100, 0.5% sodium deoxycholate [DOC], and 0.5% SDS) was added to sheared chromatin to 1× dilution and Myc, Flag, and H3K9me3 antibodies were individually added at 5 μg per IP, incubated at 4°C for 4 h. 50 μl anti-mouse, for Myc and Flag (11201D; Life Technologies), or anti-rabbit, for H3K9me3 (11203D; Life Technologies), magnetic beads were added and incubation continued overnight at 4°C. IPs were washed 2× with 1×

Toyama et al.
Age mosaicism within nuclei of postmitotic cells

Journal of Cell Biology
https://doi.org/10.1083/jcb.201809123

441

IP buffer, washed 1× in DOC buffer (10 mM Tris, pH 8.0, 0.25 M LiCl, 0.5% NP-40, 0.5% DOC, and 1 mM EDTA), 1× in TE (10 mM Tris, pH 8.0, and 1 mM EDTA), and incubated for 20 min at RT with 150 µl elution buffer (1% SDS and 0.1 M NaHCO$_3$). Supernatant was collected, RNase A was added to 0.2 mg/ml and incubated at 37°C for 30 min, and proteinase K (50 µg/ml), EDTA (to 10 mM), and Tris, pH 6.5 (to 40 mM) were added and incubated over ight at 65°C. Input chromatin was similarly treated with RNase and proteinase K. DNA was then purified using MinElute columns (28006; Qiagen) using the Qiagen protocol, and Illumina-compatible libraries were generated using the Kapa Hyper Prep Kit (KK8504; Kapa Biosystems). Multiplexed single-end sequencing was performed on a NextSeq 500 instrument (Illumina). Domains of new histone incorporation were first defined using RSEG (Song and Smith, 2011) and metagene plots made using ngs.plot (https://github.com/shenlab-sinai/ngsplot).

Western blotting
Lysates were made from cells treated with or without doxycycline for 3 d by scraping in SDS lysis buffer (4% SDS and 100 mM Tris, pH 6.8). Lysates were quantified, and 30 µg protein was loaded on 4–12% Bis-Tris gradient gels (Invitrogen). Wet transfers were performed onto nitrocellulose paper (Protran NC; GE Healthcare Biosciences), blocked with 5% milk, and incubated with the previously described antibodies for 1 h. Blots were washed 3× for 5 min using TBST (0.25% Tween 20, 20 mM Tris, pH 8.0, and 137 mM NaCl) and incubated with HRP secondary antibody for 1 h. Blots were then washed 3× for 5 min and developed using SuperSignal West Pico or Femto (PI34078, PI34095; Thermo Fisher Scientific) reagent and exposure to film.

mRNA levels
Lysates were made from cells treated with or without doxycycline for 3 d, and total RNA was purified using the RNeasy Mini Kit (Qiagen). From this, 250 µg RNA was used to make cDNA using the QuantiTect Reverse transcription kit (Qiagen). PCR reactions using primers amplifying ~200-bp fragments of GAPDH and Pom121 from 1 µl cDNA were set up, and samples were taken at 26, 30, 32, and 35 cycles. Samples were run on 2% agarose gels stained with ethidium bromide and imaged. Primers used were as follows: GAPDH (5′-GGAAGGGCTCATGACCACAGTCC, CATCATACTTGGCAGGTTTCTCCAGGCGG-3′) and Pom121 (5′-CCAGGAGAAAAGGTTACAGATACAACC, GGAAGCATCATCTGG CTTGTCCTCC-3′).

Correlative EM and MIMS
Before image acquisition, mice were metabolically labeled with ^{15}N as described (Toyama et al., 2013) and chased with regular chow that contains the natural abundance of ^{14}N for 6 mo. Next, the animals were euthanized, perfused with fixative (0.15 M cacodylate buffer [Ted Pella], pH 7.4, containing 2.5% glutaraldehyde [Electron Microscopy Sciences], 2% formaldehyde [fresh from paraformaldehyde; EMS] with 2 mM calcium chloride at 35°C for 5 min), and the brain was dissected and prepared for EM imaging as in Deerinck et al. (2010). Next, using a scanning electron microscope (MerlinSEM; Zeiss), we acquired high-resolution electron micrographs (pixel size <4 nm) and recorded the tissue coordinates of en face NPCs for individual neurons (n = 4) from one mouse in 80-nm-thick sections mounted on ~7 × 7-mm silicon wafers. Next, the silicon wafers were mounted on MIMS sample holders and processed for MIMS mapping. MIMS acquisition of mapped neuronal NPCs was done as described previously (Zhang et al., 2012). Briefly, NPCs imaged and mapped previously were scanned with a NanoSIMS 50L (Cameca) using a Cesium (Cs$^-$) beam with a spot size of ~110 nm, and ^{15}N and ^{14}N levels were detected simultaneously with a pixel dwell time of 3–10 ms/pixel in 30–60-µm raster using a 512 × 512 or 1,024 × 1,024 image size (Zhang et al., 2012). Overlay of MIMS and SEM images was done using linear alignment tools developed in house (National Center for Microscopy and Imaging Research). Quantification of MIMS ^{15}N, ^{14}N, and ^{15}N/^{14}N ratio data were done with the Fiji plugin OpenMIMS (Harvard; Zhang et al., 2012).

Online supplemental material
Fig. S1 provides information about the localization bias between RITE-tagged constructs. Fig. S2 provides details about NPC turnover in nondividing C2C12 quiescent cells and shows NPC replacement expressed in nuclear pore density. Fig. S3 provides information about tissue sectioning and image acquisition for MIMS and data about NPC replacement in quiescent cells.

Acknowledgments

Author contributions: B.H. Toyama and M.W. Hetzer conceived and directed the project. B.H. Toyama adapted the RITE

system and performed and analyzed all experiments described with the following exception. V. Lev-Ram performed the ^{15}N pulse chase of mice, T.J. Deerinck imaged the tissue by SEM, and R. Arrojo e Drigo mapped the tissue with MIMS and performed image analysis with R. Ramachandra, under the guidance of M.H. Ellisman and C. Lechene. B.H. Toyama, R. Arrojo e Drigo and M.W. Hetzer wrote the manuscript.

References

Alber, A.B., E.R. Paquet, M. Biserni, F. Naef, and D.M. Suter. 2018. Single live cell monitoring of protein turnover reveals intercellular variability and cell-cycle dependence of degradation rates. *Mol. Cell.* 71:1079–1091.e9. https://doi.org/10.1016/j.molcel.2018.07.023

Antonin, W., C. Franz, U. Haselmann, C. Antony, and I.W. Mattaj. 2005. The integral membrane nucleoporin pom121 functionally links nuclear pore complex assembly and nuclear envelope formation. *Mol. Cell.* 17:83–92. https://doi.org/10.1016/j.molcel.2004.12.010

Aygün, O., S. Mehta, and S.I.S. Grewal. 2013. HDAC-mediated suppression of histone turnover promotes epigenetic stability of heterochromatin. *Nat. Struct. Mol. Biol.* 20:547–554. https://doi.org/10.1038/nsmb.2565

Bergmann, O., R.D. Bhardwaj, S. Bernard, S. Zdunek, F. Barnabé-Heider, S. Walsh, J. Zupicich, K. Alkass, B.A. Buchholz, H. Druid, et al. 2009. Evidence for cardiomyocyte renewal in humans. *Science.* 324:98–102. https://doi.org/10.1126/science.1164680

Blau, H.M., B.D. Cosgrove, and A.T.V. Ho. 2015. The central role of muscle stem cells in regenerative failure with aging. *Nat. Med.* 21:854–862. https://doi.org/10.1038/nm.3918

Bloemendal, H., W. de Jong, R. Jaenicke, N.H. Lubsen, C. Slingsby, and A. Tardieu. 2004. Ageing and vision: structure, stability and function of lens crystallins. *Prog. Biophys. Mol. Biol.* 86:407–485. https://doi.org/10.1016/j.pbiomolbio.2003.11.012

Campeau, E., V.E. Ruhl, F. Rodier, C.L. Smith, B.L. Rahmberg, J.O. Fuss, J. Campisi, P. Yaswen, P.K. Cooper, and P.D. Kaufman. 2009. A versatile viral system for expression and depletion of proteins in mammalian cells. *PLoS One.* 4:e6529. https://doi.org/10.1371/journal.pone.0006529

D'Angelo, M.A., M. Raices, S.H. Panowski, and M.W. Hetzer. 2009. Age-dependent deterioration of nuclear pore complexes causes a loss of nuclear integrity in postmitotic cells. *Cell.* 136:284–295. https://doi.org/10.1016/j.cell.2008.11.037

Deerinck, T.J., E. Bushong, A. Thor, and M.H. Ellisman. 2010. NCMIR methods for 3D EM: A new protocol for preparation of biological specimens for serial block face scanning electron microscopy. *National Center for Microscopy and Imaging Research.* 6–8.

Doucet, C.M., J.A. Talamas, and M.W. Hetzer. 2010. Cell cycle-dependent differences in nuclear pore complex assembly in metazoa. *Cell.* 141:1030–1041. https://doi.org/10.1016/j.cell.2010.04.036

Fellmann, C., T. Hoffmann, V. Sridhar, B. Hopfgartner, M. Muhar, M. Roth, D.Y. Lai, I.A.M. Barbosa, J.S. Kwon, Y. Guan, et al. 2013. An optimized microRNA backbone for effective single-copy RNAi. *Cell Reports.* 5:1704–1713. https://doi.org/10.1016/j.celrep.2013.11.020

Fischer, C.A., and P. Morell. 1974. Turnover of proteins in myelin and myelin-like material of mouse brain. *Brain Res.* 74:51–65. https://doi.org/10.1016/0006-8993(74)90111-5

Fonck, E., G.G. Feigl, J. Fasel, D. Sage, M. Unser, D.A. Rüfenacht, and N. Stergiopulos. 2009. Effect of aging on elastin functionality in human cerebral arteries. *Stroke.* 40:2552–2556. https://doi.org/10.1161/STROKEAHA.108.528091

Hake, S.B., B.A. Garcia, E.M. Duncan, M. Kauer, G. Dellaire, J. Shabanowitz, D.P. Bazett-Jones, C.D. Allis, and D.F. Hunt. 2006. Expression patterns and post-translational modifications associated with mammalian histone H3 variants. *J. Biol. Chem.* 281:559–568. https://doi.org/10.1074/jbc.M509266200

Haus, J.M., J.A. Carrithers, S.W. Trappe, and T.A. Trappe. 2007. Collagen, cross-linking, and advanced glycation end products in aging human skeletal muscle. *J. Appl. Physiol.* 103:2068–2076. https://doi.org/10.1152/japplphysiol.00670.2007

Ibarra, A., and M.W. Hetzer. 2015. Nuclear pore proteins and the control of genome functions. *Genes Dev.* 29:337–349. https://doi.org/10.1101/gad.256495.114

Jackson, V. 1990. In vivo studies on the dynamics of histone-DNA interaction: evidence for nucleosome dissolution during replication and transcription and a low level of dissolution independent of both. *Biochemistry.* 29:719–731. https://doi.org/10.1021/bi00455a019

Kimura, H., and P.R. Cook. 2001. Kinetics of core histones in living human cells: little exchange of H3 and H4 and some rapid exchange of H2B. *J. Cell Biol.* 153:1341–1353. https://doi.org/10.1083/jcb.153.7.1341

Kireeva, M.L., W. Walter, V. Tchernajenko, V. Bondarenko, M. Kashlev, and V.M. Studitsky. 2002. Nucleosome remodeling induced by RNA polymerase II: loss of the H2A/H2B dimer during transcription. *Mol. Cell.* 9:541–552. https://doi.org/10.1016/S1097-2765(02)00472-0

Knott, S.R.V., A. Maceli, N. Erard, K. Chang, K. Marran, X. Zhou, A. Gordon, O.E. Demerdash, E. Wagenblast, S. Kim, et al. 2014. A computational algorithm to predict shRNA potency. *Mol. Cell.* 56:796–807. https://doi.org/10.1016/j.molcel.2014.10.025

Kvam, E., and D.S. Goldfarb. 2007. Nucleus-vacuole junctions and piecemeal microautophagy of the nucleus in S. cerevisiae. *Autophagy.* 3:85–92. https://doi.org/10.4161/auto.3586

Lynnerup, N., H. Kjeldsen, S. Heegaard, C. Jacobsen, and J. Heinemeier. 2008. Radiocarbon dating of the human eye lens crystallines reveal proteins without carbon turnover throughout life. *PLoS One.* 3:e1529. https://doi.org/10.1371/journal.pone.0001529

Masters, P.M., J.L. Bada, and J.S. Zigler Jr. 1977. Aspartic acid racemisation in the human lens during ageing and in cataract formation. *Nature.* 268:71–73. https://doi.org/10.1038/268071a0

Maze, I., W. Wenderski, K.M. Noh, R.C. Bagot, N. Tzavaras, I. Purushothaman, S.J. Elsässer, Y. Guo, C. Ionete, Y.L. Hurd, et al. 2015. Critical Role of Histone Turnover in Neuronal Transcription and Plasticity. *Neuron.* 87:77–94. https://doi.org/10.1016/j.neuron.2015.06.014

Mertens, J., A.C.M. Paquola, M. Ku, E. Hatch, L. Böhnke, S. Ladjevardi, S. McGrath, B. Campbell, H. Lee, J.R. Herdy, et al. 2015. Directly Reprogrammed Human Neurons Retain Aging-Associated Transcriptomic Signatures and Reveal Age-Related Nucleocytoplasmic Defects. *Cell Stem Cell.* 17:705–718. https://doi.org/10.1016/j.stem.2015.09.001

Mito, Y., J.G. Henikoff, and S. Henikoff. 2005. Genome-scale profiling of histone H3.3 replacement patterns. *Nat. Genet.* 37:1090–1097. https://doi.org/10.1038/ng1637

Olmos, Y., L. Hodgson, J. Mantell, P. Verkade, and J.G. Carlton. 2015. ESCRT-III controls nuclear envelope reformation. *Nature.* 522:236–239. https://doi.org/10.1038/nature14503

Ori, A., B.H. Toyama, M.S. Harris, T. Bock, M. Iskar, P. Bork, N.T. Ingolia, M.W. Hetzer, and M. Beck. 2015. Integrated Transcriptome and Proteome Analyses Reveal Organ-Specific Proteome Deterioration in Old Rats. *Cell Syst.* 1:224–237. https://doi.org/10.1016/j.cels.2015.08.012

Petersen, K.F., D. Befroy, S. Dufour, J. Dziura, C. Ariyan, D.L. Rothman, L. DiPietro, G.W. Cline, and G.I. Shulman. 2003. Mitochondrial dysfunction in the elderly: possible role in insulin resistance. *Science.* 300:1140–1142. https://doi.org/10.1126/science.1082889

Rabut, G., V. Doye, and J. Ellenberg. 2004. Mapping the dynamic organization of the nuclear pore complex inside single living cells. *Nat. Cell Biol.* 6:1114–1121. https://doi.org/10.1038/ncb1184

Retz, K.C., and W.J. Steele. 1980. Ribosome turnover in rat brain and liver. *Life Sci.* 27:2601–2604. https://doi.org/10.1016/0024-3205(80)90546-9

Roberts, P., S. Moshitch-Moshkovitz, E. Kvam, E. O'Toole, M. Winey, and D.S. Goldfarb. 2003. Piecemeal microautophagy of nucleus in Saccharomyces cerevisiae. *Mol. Biol. Cell.* 14:129–141. https://doi.org/10.1091/mbc.e02-08-0483

Sarkar, S., J.E. Davies, Z. Huang, A. Tunnacliffe, and D.C. Rubinsztein. 2007. Trehalose, a novel mTOR-independent autophagy enhancer, accelerates the clearance of mutant huntingtin and α-synuclein. *J. Biol. Chem.* 282:5641–5652. https://doi.org/10.1074/jbc.M609532200

Savas, J.N., B.H. Toyama, T. Xu, J.R. Yates, and M.W. Hetzer. 2012. Extremely long-lived nuclear pore proteins in the rat brain. *Science.* 335:942. https://doi.org/10.1126/science.1217421

Shapiro, S.D., S.K. Endicott, M.A. Province, J.A. Pierce, and E.J. Campbell. 1991. Marked longevity of human lung parenchymal elastic fibers deduced from prevalence of D-aspartate and nuclear weapons-related radiocarbon. *J. Clin. Invest.* 87:1828–1834. https://doi.org/10.1172/JCI115204

Song, Q., and A.D. Smith. 2011. Identifying dispersed epigenomic domains from ChIP-Seq data. *Bioinformatics.* 27:870–871. https://doi.org/10.1093/bioinformatics/btr030

Spalding, K.L., R.D. Bhardwaj, B.A. Buchholz, H. Druid, and J. Frisén. 2005. Retrospective birth dating of cells in humans. *Cell.* 122:133–143. https://doi.org/10.1016/j.cell.2005.04.028

Taylor, R.C., and A. Dillin. 2011. Aging as an event of proteostasis collapse. *Cold Spring Harb. Perspect. Biol.* 3:a004440. https://doi.org/10.1101/cshperspect.a004440

Toyama, B.H., and M.W. Hetzer. 2013. Protein homeostasis: live long, won't prosper. *Nat. Rev. Mol. Cell Biol.* 14:55–61. https://doi.org/10.1038/nrm3496

Toyama, B.H., J.N. Savas, S.K. Park, M.S. Harris, N.T. Ingolia, J.R. Yates III, and M.W. Hetzer. 2013. Identification of long-lived proteins reveals exceptional stability of essential cellular structures. *Cell.* 154:971–982. https://doi.org/10.1016/j.cell.2013.07.037

Verzijl, N., J. DeGroot, S.R. Thorpe, R.A. Bank, J.N. Shaw, T.J. Lyons, J.W. Bijlsma, F.P. Lafeber, J.W. Baynes, and J.M. TeKoppele. 2000. Effect of collagen turnover on the accumulation of advanced glycation end products. *J. Biol. Chem.* 275:39027–39031. https://doi.org/10.1074/jbc.M006700200

Verzijlbergen, K.F., V. Menendez-Benito, T. van Welsem, S.J. van Deventer, D.L. Lindstrom, H. Ovaa, J. Neefjes, D.E. Gottschling, and F. van Leeuwen. 2010. Recombination-induced tag exchange to track old and new

proteins. *Proc. Natl. Acad. Sci. USA.* 107:64–68. https://doi.org/10.1073/pnas.0911164107

Webster, B.M., P. Colombi, J. Jäger, and C.P. Lusk. 2014. Surveillance of nuclear pore complex assembly by ESCRT-III/Vps4. *Cell.* 159:388–401. https://doi.org/10.1016/j.cell.2014.09.012

Woulfe, J., D.A. Gray, and I.R.A. Mackenzie. 2010. FUS-immunoreactive intranuclear inclusions in neurodegenerative disease. *Brain Pathol.* 20:589–597. https://doi.org/10.1111/j.1750-3639.2009.00337.x

Yang, Y.P., L.F. Hu, H.F. Zheng, C.J. Mao, W.D. Hu, K.P. Xiong, F. Wang, and C.F. Liu. 2013. Application and interpretation of current autophagy inhibitors and activators. *Acta Pharmacol. Sin.* 34:625–635. https://doi.org/10.1038/aps.2013.5

Zhang, D.S., V. Piazza, B.J. Perrin, A.K. Rzadzinska, J.C. Poczatek, M. Wang, H.M. Prosser, J.M. Ervasti, D.P. Corey, and C.P. Lechene. 2012. Multi-isotope imaging mass spectrometry reveals slow protein turnover in hair-cell stereocilia. *Nature.* 481:520–524. https://doi.org/10.1038/nature10745

Zhang, K., J. Sha, and M.L. Harter. 2010. Activation of Cdc6 by MyoD is associated with the expansion of quiescent myogenic satellite cells. *J. Cell Biol.* 188:39–48. https://doi.org/10.1083/jcb.200904144